

Prediction of 1:1 Kagome Metals with Superconductivity and Nontrivial Band Topology

Na Jiao,^{1,*} Shu-Xiang Qiao¹,^{*} Pan Zhou,² Hong-Yan Lu,^{1,†} and Ping Zhang^{1,3}

¹*School of Physics and Physical Engineering, Qufu Normal University, Qufu 273165, China*

²*Hunan Provincial Key laboratory of Thin Film Materials and Devices,*

School of Materials Science and Engineering, Xiangtan University, Xiangtan 411105, China

³*Institute of Applied Physics and Computational Mathematics, Beijing 100088, China*

Kagome superconductors featuring topologically nontrivial band structures have attracted extensive research interest. FeSn and CoSn is a new kind of kagome material with intrinsic magnetism, which suppresses the emergence of superconductivity. Here, we theoretically predict a new kind of 1:1 kagome MSn (M =transition metal), which exhibit intrinsic superconductivity and nontrivial band topology by first-principles calculations. Among twenty-seven candidates, MSn (M = Mo, Hf, Nb, Ta, W, Ti) are theoretically identified as both dynamically and thermodynamically stable. And, five non-magnetic MSn (M = Mo, Hf, Nb, Ta, W) exhibit phonon-mediated superconductivity. Especially, the d orbitals bands display Dirac points and van Hove singularities near the Fermi level, which contribute to the emergence of topology and the electron-phonon coupling (EPC). More interestingly, MoSn, HfSn and NbSn show nontrivial topological band structure at the Fermi level. Thus, the predicted MSn establish a platform integrating superconductivity and topological order.

I. INTRODUCTION

Kagome-lattice materials represent a frontier in condensed matter physics, as their characteristic corner-sharing triangular geometry naturally hosts flat bands [1], van Hove singularities [2–4], Dirac fermions [5], and topological band structures [6–9], stabilizing diverse quantum ground states including magnetism [10–12], charge density waves [13–16], nontrivial topology [8, 16], and superconductivity [16–18]. In recent years, a large number of kagome compounds have been theoretically predicted and experimentally synthesized, such as 1:1 type CoSn [19, 20], FeSn [11, 12] and FeGe [21–23], 1:3 type MB_3 (M = B, Be, Ca, Sr, Mn) [24–26], 1:5 type MPd_5 (M = Ca, Sr, Ba) [9], 3:1 type Mn_3X (X = Sn, Ge, Ga) [27] and Ni_3Sn [28], 1:3:5 type AV_3Sb_5 (A = K, Rb, Cs) [7, 14, 17, 18, 29]. The ground of these systems exhibit highly distinct ground state properties.

Most kagome materials exhibit rich magnetic properties. For instance, FeSn is an antiferromagnetic metal [12], Mn_3X (X = Sn, Ge, Ga) possesses a breathing kagome lattice with noncollinear antiferromagnetic order [27], and $Co_3Sn_2S_2$ is a ferromagnetic Weyl semimetal [30]. Intrinsic superconductivity has been discovered in many kagome materials, including MgB_3 [24], MPd_5 (M = Ca, Sr, Ba) [9], and YT_6Sn_6 [8]. The coexistence of intrinsic phonon-mediated superconductivity and nontrivial topology in MPd_5 offering a new avenue to investigate the fundamental physics of topological superconductivity in kagome systems. Especially, in the kagome superconductor CsV_3Sb_5 , anomalous Hall effect appears concurrently with the the higher-temperature charge density wave transition, making this system an ideal platform

for studying the interplay among nontrivial topology, charge-density-wave, and superconductivity [31]. The coexistence of nontrivial topology and superconductivity in these materials makes them promising candidates for exploring topological superconductivity.

Recently, 1:1 type kagome materials, characterized by their simple structure, high symmetry, and clear physical picture, serve as prototypical platforms for exploring the intrinsic electronic states of kagome lattices. However, all available studies show that conventional 1:1 type kagome materials are only paramagnetic [19] or antiferromagnetic metals [12], lacking both intrinsic superconductivity. The coexistence of topology and superconductivity has never been achieved in 1:1 type kagome lattices, representing a critical gap limiting the development of this field. Although 1:3, 1:5, 1:3:5, and other families have realized the coexistence of superconductivity and topology properties [9, 18, 24], the missing quantum states in ideal 1:1 type kagome systems prevent a complete understanding of the intrinsic correlations among electron-phonon coupling, topological and superconductivity, and hinder the establishment of universal design principles for kagome quantum materials.

In this Letter, we predict that 1:1 kagome materials, MSn (M = transition metals), exhibit both intrinsic superconductivity and nontrivial topological features. Among the twenty-seven 1:1 kagome MSn candidates, five are non-magnetic and thermodynamically as well as dynamically stable, all exhibiting phonon-mediated superconductivity. The d -orbital bands display Dirac points and VHSs near the Fermi level, which contribute to the emergence of topology and the electron-phonon coupling (EPC). Moreover, three of them satisfy the criteria for topological metals. Therefore, these pristine MSn materials integrate Cooper pairing with nontrivial surface states, thereby eliminating the need for external doping or heterostructure engineering. These findings not only enrich the properties of the kagome family but

* E-mail: j_n2013@126.com

† E-mail: hylu@qfnu.edu.cn

also establish 1:1 kagome lattice materials as a promising platform for exploring the interplay between topology and superconductivity.

II. COMPUTATIONAL METHODS

The structural relaxation and electronic property calculations are performed within the framework of density functional theory (DFT) using the Vienna ab-initio Simulation Package (VASP) [32] and the QUANTUM ESPRESSO (QE) package [33]. Phonon spectra and EPC calculations are carried out using density functional perturbation theory (DFPT) [34, 35] as implemented in QE. The exchange-correlation functional is treated using the generalized gradient approximation (GGA) with the Perdew-Burke-Ernzerhof (PBE) parametrization [36]. Electron-ion interactions are modeled using the projector augmented-wave (PAW) approach [37]. In the calculation, the wave function and charge density cutoff energy are 80 and 800 Ry, respectively. $6 \times 6 \times 8$ k -point grid is used for charge self consistent calculation, and a $3 \times 3 \times 4$ q -point grid for dynamical matrix. For DOS calculations, $18 \times 18 \times 24$ k -point grid is used. The surface states are obtained using the iterative Green's function approach, implemented in the WANNIERTOOLS package [38, 39], based on maximally localized Wannier functions (MLWFs) [40, 41] generated via the VASP2WANNIER90 interface [42]. Additional computational details are provided in the Supplemental Material (SM) [43] (see also references [44–46] therein).

III. RESULTS AND DISCUSSIONS

A. Crystal structure and stability

The structure of MSn (M =transition metal) is based on the experimentally synthesized FeSn [11]. Figure 1(a) shows the crystal structure of MSn , where the M (transition-metal) atoms form the kagome lattice. The primitive cell contains equal numbers of transition-metal M and Sn atoms with 1:1 ratio. The Sn atoms occupy two inequivalent lattice sites, labeled Sn₁ and Sn₂ in Fig. 1(a), lying at the hexagonal center of the M -kagome layer and above the triangular sites, respectively, as shown in Fig. 1(b). The space group of 1:1 kagome compound MSn is $P6/mmm$ (No. 191), which incorporates kagome, triangular, and hexagonal layers, which are expected to give rise to intriguing physical properties. Figure 1(c) shows the Brillouin zone and the surface Brillouin zone projection of the MSn structure. As mentioned above, FeSn and CoSn exhibit magnetic ordering and cannot display superconductivity. Atomic substitution is a widely employed strategy for the design and synthesis of new materials. Therefore, we intend to substitute Fe or Co atoms with other transition metal elements to design and identify potential superconducting

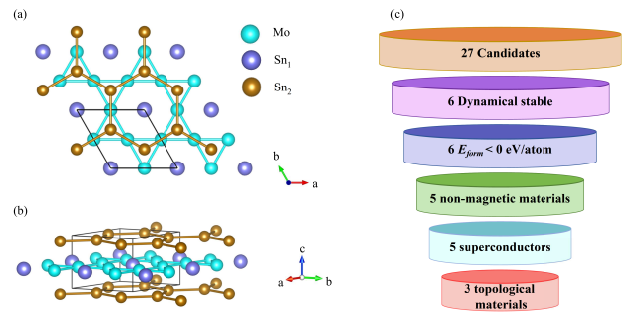


FIG. 1. Top (a) and side (b) views of the crystal structure of MSn (M =transition metals). (c) Schematic diagram of the screening process of MSn .

TABLE I. The lattice constants a (Å), c (Å), and formation energy E_{form} (eV/atom) of stable MSn ($M = \text{Mo, Hf, Nb, Ta, W, Ti}$).

Materials	a	c	E_{form}
MoSn	5.61	4.72	-0.107
HfSn	6.04	4.97	-0.138
NbSn	5.80	4.84	-0.076
TaSn	5.78	4.84	-0.079
WSn	5.61	4.75	-0.293
TiSn	5.71	4.81	-0.244

and topological materials. Here, we systematically constructed twenty-seven MSn structures by substituting Fe or Co with other transition metal elements. As shown in the flowchart in Fig. 1(c), the dynamic and thermodynamic stability of the MSn structures are verified using phonon spectrum and formation energy (E_{form}) calculations, respectively. The formation energy is defined as $E_{form} = [E_{MSn} - (3E_M + 3E_{Sn})]/6$, where E_{MSn} , E_M and E_{Sn} denote the total energies of 1:1 kagome materials MSn structure, the simple substance of M , and the Sn crystal (space group Im3m), respectively. The absence of imaginary phonon frequencies, as shown in Fig. S1 [43], demonstrates the dynamic stability, while the negative formation energies listed in Table I indicate the thermodynamic stability of these structures. Consequently, MSn ($M = \text{Mo, Hf, Nb, Ta, W, Ti}$) are dynamically and thermodynamically stable, among which TiSn is found to exhibit magnetic properties and MSn ($M = \text{Mo, Hf, Nb, Ta, W}$) possess non-magnetic metal properties. Therefore, the following sections mainly focus on investigating the electronic properties of these non-magnetic metal materials, including their superconductivity and electronic topology. These results are summarized in Fig. 1(c). The optimized lattice parameters (a and c) and formation energies (E_{form}) of the six stable MSn ($M = \text{Mo, Hf, Nb, Ta, W, Ti}$) are also listed in Table I, which may serve as a reference for future exper-

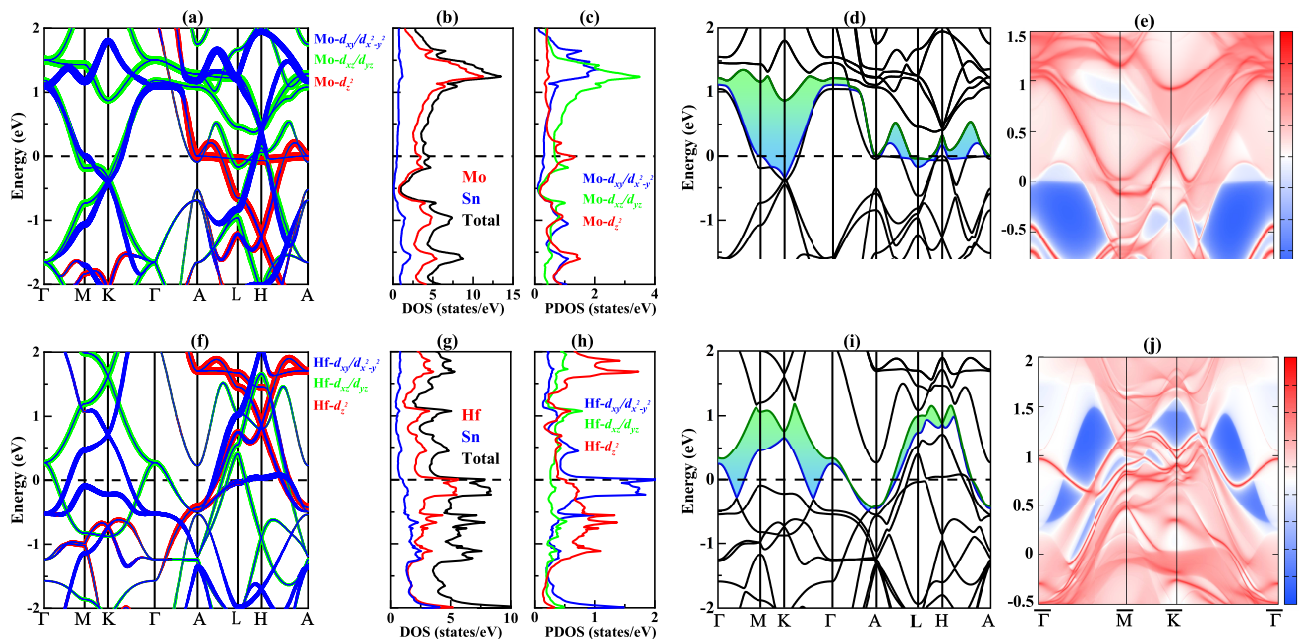


FIG. 2. (a) Orbital-projected electronic band structure without SOC, (b) total DOS, (c) PDOS, (d) band structure with SOC, and (e) surface states of MoSn. (f) to (j) are similar to (a) to (e), but for HfSn.

imental synthesis and characterization. The experimental realization of the predicted MSn maybe can prepare via high-temperature solution growth methods, analogous to those successfully employed in the synthesis of related compounds such as FeSn[11] and FeGe [47]. Given the structural and chemical similarities among these systems—particularly their formation through metal-rich flux environments—the self-flux method presents a feasible and straightforward route for obtaining single crystals of MSn . In this approach, Sn can serve as both the reactive component and the solvent (flux), facilitating the controlled crystallization of the target phase under equilibrium conditions. This class of synthesis strategies has proven effective for kagome metallic.

B. Electronic and topological properties

To understand the novel properties of kagome materials, analyzing their electronic structures is essential. Figure 2 presents the calculated electronic structures and band topology of MoSn and HfSn. The band structures of MoSn and HfSn exhibit Dirac points at the K point, VHSs at the M point, and flat-band-like bands along the A - L - H - A path near the Fermi level. As can be seen from Figs. 2(b) and 2(g), the density of states near the Fermi level is primarily contributed by M atoms, with a very small contribution from Sn atoms. Therefore, the weak interlayer coupling results in the DOS near the Fermi level being predominantly contributed by M atoms, and the d -orbitals of M atoms exhibit localization near the Fermi level. According to the projected band structures

and orbital projected densities of states (PDOS) shown in Figs. 2(a)-2(c) and 2(f)-2(h), the flat-band-like bands in MoSn originate mainly from Mo- d_{z^2} orbitals, while those in HfSn are primarily derived from Hf- $d_{xy}/d_{x^2-y^2}$ orbitals. As shown in Figs. 2(a) and 2(f), both MoSn and HfSn exhibit Dirac points at the K point, which are mainly contributed by Mo- d_{xz}/d_{yz} and Hf- $d_{xy}/d_{x^2-y^2}$ orbitals, respectively. The four VHSs (saddle points) at the M point are also primarily derived from these two types of orbitals. The energy bands, total DOS, and PDOS of the other three superconducting materials are shown in Fig. S2 [43], all of which exhibit metallic behavior. Compared with the other MSn materials, the saddle-point VHSs of MoSn and HfSn lie much closer to the Fermi level, leading to an enhanced DOS that may promote superconductivity [48].

The possible topological characteristics of the superconducting MSn are analyzed via calculations of the \mathbb{Z}_2 topological invariant, Wannier charge centers (WCCs), and surface states [16]. Our calculations reveal that three of the five superconducting materials (MoSn, HfSn, and NbSn) possess nontrivial topological characteristics. The electronic band structures with SOC for these three materials are shown in Figs. 2(d), 2(i), and Fig. S3 [43]. The bands near the Fermi level form continuous energy gaps throughout the Brillouin zone upon inclusion of SOC, as highlighted in Figs. 2(d), 2(i), and Fig. S3 [43]. The continuous energy gaps enable the determination of the \mathbb{Z}_2 topological invariant, defined in the same manner as in Bi₂Se₃ [49].

The \mathbb{Z}_2 topological invariant is subsequently calculated using the WCC method. For these three materials, an ar-

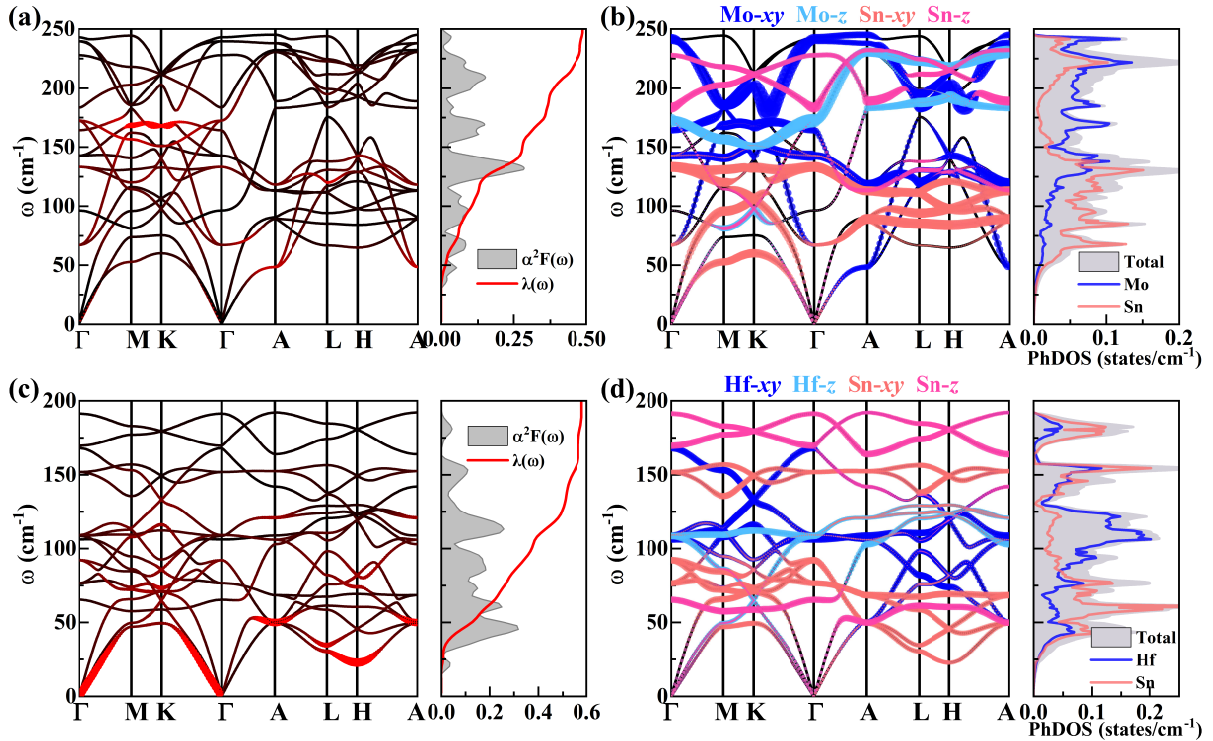


FIG. 3. (a) Phonon dispersion weighted by the magnitude of $\lambda_{\mathbf{q}\nu}$ (EPC for phonon mode $\mathbf{q}\nu$), Eliashberg spectral function $\alpha^2 F(\omega)$, and EPC $\lambda(\omega)$, (b) phonon dispersion weighted by the vibration modes of each atom and PhDOS for VSn. (c) to (d) are similar to (a) to (b), but for HfSn.

bitrary horizontal reference line intersects the WCC evolution curves an odd number of times, indicating the \mathbb{Z}_2 value of 1, as shown in Fig. S4 [43]. Similar to other kagome metals such as $YT_6\text{Sn}_5$ [8] and MPd_5 [9], MoSn, HfSn, and NbSn preserve both spatial inversion and time-reversal symmetries. Figures 2(e), 2(j), and Fig. S3 illustrate the (001) surface states of MoSn, HfSn, and NbSn, and it is found that there are prominent surface states near the Fermi level. These surface states clearly cross the Fermi level, suggesting potential avenues for realizing topological superconductivity. The presence of nontrivial topological surface states within the bulk gap further supports the nontrivial band topology of these materials. Therefore, MoSn, HfSn, and NbSn exhibit nontrivial topological band properties and can be classified as topological metals.

C. EPC and superconductivity

Given that $M\text{Sn}$ ($M = \text{Mo, Hf, Nb, Ta, W}$) exhibit non-magnetic metallic properties and flat band characteristics, we further explore their potential for superconductivity. As mentioned in the previous section, the flat bands of MoSn and HfSn are located at the Fermi level, resulting in high DOS, which enhances the EPC and promotes stronger superconductivity. Furthermore, we calculated the phonon dispersion weighted by the magni-

tude of EPC linewidth $\lambda_{\mathbf{q}\nu}$, Eliashberg spectral function $\alpha^2 F(\omega)$, EPC $\lambda(\omega)$, phonon dispersion weighted by the vibration modes contributed by different elements, and phonon DOS (PhDOS) of MoSn and HfSn, as shown in Fig. 3. For kagome materials $M\text{Sn}$, the primitive cell contains six atoms, giving rise to eighteen phonon branches, including three acoustic and fifteen optical modes.

To analyze the phonon mode contributions to the superconducting mechanism in MoSn and HfSn, we compare the phonon dispersions associated with different atomic vibration modes (Figs. 3(a), 3(c)) and the distribution and strength of the EPC (Figs. 3(b), 3(d)). For MoSn, the vibration modes near the M and K points (around 170 cm^{-1}) exhibit significant EPC effects, resulting in a pronounced enhancement of the EPC λ . The intermediate-frequency phonon modes ($130\text{-}170 \text{ cm}^{-1}$) contribute approximately 56 % to the total EPC constant λ . As shown in Fig. 3(b), due to the difference in atomic masses, the atomic vibration frequencies exhibit a relatively separation. The vibrations of Mo atoms are primarily concentrated in the high-frequency region, whereas the vibrations of Sn atoms dominate the low-frequency region. Through comparison, the dominant EPC contributions arise mainly from the Mo-xy plane vibration modes. Vibrations in other frequency ranges are also distributed throughout the spectrum and make additional contributions to the EPC.

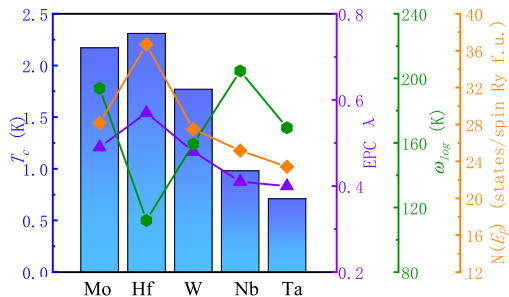


FIG. 4. Variation of T_c , EPC λ , ω_{log} , and $N(E_F)$ for superconducting MSn .

For HfSn, as shown in Fig. 3(c), the EPC mainly originates from low-frequency vibrations ($0-100 \text{ cm}^{-1}$), which contribute approximately 71 % to the total EPC constant λ . The vibrational frequency distributions of Hf and Sn atoms are shown in Fig. 3(d). It is observed that the vibrations of Sn atoms are mainly concentrated in the low-frequency region, and the phonon mode dominated by the Sn- xy plane vibrations shows pronounced softening near the H point, which strongly contributes to the enhanced EPC strength. Similar to MoSn, vibrations in other frequency ranges also contribute to the EPC, though to a lesser extent. The EPC calculation results for the other three superconducting MSn are shown in Fig. S4 [43].

According to our calculations, the total EPC constants λ for MoSn and HfSn are 0.49 and 0.57, respectively, indicating that both materials can be categorized as weak coupling superconductors. The calculated superconducting T_c are 2.17 K for MoSn and 2.31 K for HfSn. In addition, the corresponding data for the other three superconducting MSn are summarized in Fig. 4 and Table S1 [43]. It is evident that the T_c values of the 1:1 kagome materials are positively correlated with the EPC λ and the DOS at the Fermi level $N(E_F)$, suggesting that they are conventional phonon-mediated superconductors. Therefore, our results provide valuable insights and op-

portunities for exploring the novel physical properties of 1:1 kagome materials.

Importantly, our calculations reveal that MoSn, HfSn, and NbSn are superconducting and topological metals (SCTMs) with coexisting superconductivity and non-trivial topological properties. Experimentally, superconductivity in topological materials is typically induced by doping topological insulators (such as Cu- or Nb-doped Bi_2Se_3 [50, 51] and $\text{Sn}_{1-x}\text{In}_x\text{Te}$ [52]) or by proximity effects in hetero-structures [53, 54]. Unlike the charge-density-wave (CDW) dominated AV_3Sb_5 ($A = \text{K}, \text{Rb}, \text{Cs}$) family, where superconductivity emerges under pressure[7], MSn exhibits intrinsic coexistence of topological band features and superconductivity. Furthermore, while FeSn [11] and FeGe [21] share a similar kagome crystal but display itinerant magnetism rather than bulk superconductivity. Similar with the recently discovered kagome superconductor YT_6Sn_6 ($T = \text{V}, \text{Rb}, \text{Ta}$) [8], MSn ($M = \text{Mo}, \text{Hf}, \text{Nb}$) achieves a rare combination of superconductivity and topological robustness without magnetic ordering. These findings may serve as valuable references for future experimental and theoretical studies.

IV. CONCLUSION

In summary, we have predicted a new class of 1:1 kagome materials, unveiling their structural stability, topological, and superconducting properties. Through comprehensive screening of twenty-seven candidate materials, we identified MSn ($M = \text{Mo}, \text{Hf}, \text{Nb}, \text{Ta}, \text{W}, \text{Ti}$) are dynamically and thermally stable. MSn ($M = \text{Mo}, \text{Hf}, \text{Nb}, \text{Ta}, \text{W}$) were further confirmed to be superconductors and the T_c ranged from 0.71 K to 2.31 K. It is worth noting that the flat-band-like and the VHSs of MoSn and HfSn are near the Fermi level, resulting in high DOS. More interestingly, MoSn, HfSn, and NbSn are identified as SCTMs, whose surface states cross the Fermi level. Thus, the predicted MSn establish a multifunctional platform integrating superconductivity and topological order without the need for external doping or hetero-structure fabrication.

V. ACKNOWLEDGEMENTS

This work is supported by the National Natural Science Foundation of China (Grant No. 12074213), the National Key R&D Program of China (Grant No. 2022YFA1403103), the Major Basic Program of Natural Science Foundation of Shandong Province (Grant No. ZR2021ZD01), and the Natural Science Foundation of Shandong Province (Grant No. ZR2023MA082).

[1] P. M. Neves, J. P. Wakefield, S. Fang, H. Nguyen, L. Ye, and J. G. Checkelsky, Crystal net catalog of model flat

band materials, *npj Comput. Mater.* **10**, 39 (2024).

- [2] Y. Hu, X. Wu, Y. Yang, S. Gao, N. C. Plumb, A. P. Schnyder, W. Xie, J. Ma, and M. Shi, Tunable topological dirac surface states and van hove singularities in kagome metal GdV_6Sn_6 , *Sci. Adv.* **8**, eadd2024 (2025).
- [3] H. D. Scammell, J. Ingham, T. Li, and O. P. Sushkov, Chiral excitonic order from twofold van hove singularities in kagome metals, *Nat. Commun.* **14**, 605 (2023).
- [4] Y. Hu, X. Wu, B. R. Ortiz, S. Ju, X. Han, J. Ma, N. C. Plumb, M. Radovic, R. Thomale, S. D. Wilson, A. P. Schnyder, and M. Shi, Rich nature of van hove singularities in kagome superconductor CsV_3Sb_5 , *Nat. Commun.* **13**, 2220 (2022).
- [5] A. Low, T. K. Bhowmik, S. Ghosh, and S. Thirupathiah, Anisotropic nonsaturating magnetoresistance observed in HoMn_6Ge_6 : A kagome dirac semimetal, *Phys. Rev. B* **109**, 195104 (2024).
- [6] P. C. Xiao, L. Yang, H. Y. Lu, N. Hao, and P. Zhang, Prediction of a kagome topological superconducting family: XB_3 ($X=\text{Ni}, \text{Pd}$), *Phys. Rev. B* **109**, 054506 (2024).
- [7] J. G. Si, W. J. Lu, Y. P. Sun, P. F. Liu, and B.-T. Wang, Charge density wave and pressure-dependent superconductivity in the kagome metal CsV_3Sb_5 : A first-principles study, *Phys. Rev. B* **105**, 024517 (2022).
- [8] L.-T. Shi, J.-G. Si, A. Liang, R. Turnbull, P.-F. Liu, and B.-T. Wang, Topological and superconducting properties in bilayer kagome metals YT_6Sn_6 ($T=\text{V}, \text{Nb}, \text{Ta}$), *Phys. Rev. B* **107**, 184503 (2023).
- [9] D. Li, Z. Wang, P. Jing, M. Shiri, K. Wang, C. Ma, S. Gong, C. Zhao, T. Wang, X. Dong, L. Zhuang, W. Liu, and Y. An, MPd_5 kagome superconductors studied by density functional calculations, *Phys. Rev. B* **111**, 144511 (2025).
- [10] L. Ye, M. Kang, J. Liu, F. von Cube, C. R. Wicker, T. Suzuki, C. Jozwiak, A. Bostwick, E. Rotenberg, D. C. Bell, L. Fu, R. Comin, and J. G. Checkelsky, Massive dirac fermions in a ferromagnetic kagome metal, *Nature* **555**, 638 (2018).
- [11] M. Kang, L. Ye, S. Fang, J. S. You, A. Levitan, M. Han, J. I. Facio, C. Jozwiak, A. Bostwick, E. Rotenberg, M. K. Chan, R. D. McDonald, D. Graf, K. Kaznatcheev, E. Vescovo, D. C. Bell, E. Kaxiras, J. van den Brink, M. Richter, M. Prasad Ghimire, J. G. Checkelsky, and R. Comin, Dirac fermions and flat bands in the ideal kagome metal FeSn , *Nat. Mater.* **19**, 163 (2020).
- [12] W. R. Meier, J. Yan, M. A. McGuire, X. Wang, A. D. Christianson, and B. C. Sales, Reorientation of antiferromagnetism in cobalt doped FeSn , *Phys. Rev. B* **100**, 184421 (2019).
- [13] X. Teng, L. Chen, F. Ye, E. Rosenberg, Z. Liu, J. X. Yin, Y. X. Jiang, J. S. Oh, M. Z. Hasan, K. J. Neubauer, B. Gao, Y. Xie, M. Hashimoto, D. Lu, C. Jozwiak, A. Bostwick, E. Rotenberg, R. J. Birgeneau, J. H. Chu, M. Yi, and P. Dai, Discovery of charge density wave in a kagome lattice antiferromagnet, *Nature* **609**, 490 (2022).
- [14] Q. Deng, H. Tan, B. R. Ortiz, A. C. Salinas, S. D. Wilson, B. Yan, and L. Wu, Coherent phonon pairs and rotational symmetry breaking of charge density wave order in the kagome superconductor CsV_3Sb_5 , *Phys. Rev. B* **112**, 125127 (2025).
- [15] M. L. Klemm, T. Zhang, B. L. Winn, F. Li, F. Ye, M. Matsuda, A. Maity, S. Xu, X. Teng, Y. Umemoto, B. Gao, M. Yi, and P. Dai, Interacting spin and charge density waves in the kagome metal FeGe , *Phys. Rev. B* **112**, 174422 (2025).
- [16] H. Tan, Y. Liu, Z. Wang, and B. Yan, Charge density waves and electronic properties of superconducting kagome metals, *Phys. Rev. Lett.* **127**, 046401 (2021).
- [17] B. R. Ortiz, L. C. Gomes, J. R. Morey, M. Winiarski, M. Bordelon, J. S. Mangum, I. W. H. Oswald, J. A. Rodriguez-Rivera, J. R. Neilson, S. D. Wilson, E. Ertekin, T. M. McQueen, and E. S. Toberer, New kagome prototype materials: discovery of KV_3Sb_5 , RbV_3Sb_5 , and CsV_3Sb_5 , *Phys. Rev. Mater.* **3**, 094407 (2019).
- [18] Y. Gu, Y. Zhang, X. Feng, K. Jiang, and J. Hu, Gapless excitations inside the fully gapped kagome superconductors AV_3Sb_5 , *Phys. Rev. B* **105**, L100502 (2022).
- [19] W. R. Meier, M.-H. Du, S. Okamoto, N. Mohanta, A. F. May, M. A. McGuire, C. A. Bridges, G. D. Samolyuk, and B. C. Sales, Flat bands in the CoSn -type compounds, *Phys. Rev. B* **102**, 075148 (2020).
- [20] H. Huang, L. Zheng, Z. Lin, X. Guo, S. Wang, S. Zhang, C. Zhang, Z. Sun, Z. Wang, H. Weng, L. Li, T. Wu, X. Chen, and C. Zeng, Flat-band-induced anomalous anisotropic charge transport and orbital magnetism in kagome metal CoSn , *Phys. Rev. Lett.* **128**, 096601 (2022).
- [21] M. Wenzel, E. Uykur, A. A. Tsirlin, S. Pal, R. M. Roy, C. Yi, C. Shekhar, C. Felser, A. V. Pronin, and M. Dressel, Intriguing low-temperature phase in the antiferromagnetic kagome metal FeGe , *Phys. Rev. Lett.* **132**, 266505 (2024).
- [22] S. Shao, J. X. Yin, I. Belopolski, J. Y. You, T. Hou, H. Chen, Y. Jiang, M. S. Hossain, M. Yahyavi, C. H. Hsu, Y. P. Feng, A. Bansil, M. Z. Hasan, and G. Chang, Intertwining of magnetism and charge ordering in kagome FeGe , *ACS Nano* **17**, 10164 (2023).
- [23] B. Zhang, J. Ji, C. Xu, and H. Xiang, Electronic and magnetic origins of unconventional charge density wave in kagome FeGe , *Phys. Rev. B* **110**, 125139 (2024).
- [24] Y. An, J. Chen, Z. Wang, J. Li, S. Gong, C. Ma, T. Wang, Z. Jiao, R. Wu, J. Hu, and W. Liu, Topological and nodal superconductor kagome magnesium triboride, *Phys. Rev. Mater.* **7**, 014205 (2023).
- [25] L. Yang, Y. P. Li, H. D. Liu, N. Jiao, M. Y. Ni, H. Y. Lu, P. Zhang, and C. S. Ting, Theoretical prediction of superconductivity in boron kagome monolayer: MB_3 ($M = \text{Be}, \text{Ca}, \text{Sr}$) and the hydrogenated CaB_3 , *Chin. Phys. Lett.* **40**, 017402 (2023).
- [26] Z. Qu, F. Han, T. Yu, M. Xu, Y. Li, and G. Yang, Boron kagome-layer induced intrinsic superconductivity in a MnB_3 monolayer with a high critical temperature, *Phys. Rev. B* **102**, 075431 (2020).
- [27] A. Zelenskiy, T. L. Monchesky, M. L. Plumer, and B. W. Southern, Anisotropic magnetic interactions in hexagonal ab -stacked kagome lattice structures: Application to Mn_3X ($X=\text{Ge}, \text{Sn}, \text{Ga}$) compounds, *Phys. Rev. B* **103**, 144401 (2021).
- [28] H. J. Kim, M. J. Kim, J. Lee, J. M. Ok, and C.-J. Kang, Tuning the flat band with in-plane biaxial strain and the emergence of superconductivity in Ni_3Sn , *Phys. Rev. B* **110**, 024504 (2024).
- [29] B. R. Ortiz, S. M. L. Teicher, Y. Hu, J. L. Zuo, P. M. Sarte, E. C. Schueller, A. M. M. Abeykoon, M. J. Krogstad, S. Rosenkranz, R. Osborn, R. Seshadri, L. Balents, J. He, and S. D. Wilson, CsV_3Sb_5 : A Z_2 topological kagome metal with a superconducting ground state, *Phys. Rev. Lett.* **125**, 247002 (2020).

- [30] D. F. Liu, A. J. Liang, E. K. Liu, Q. N. Xu, Y. W. Li, C. Chen, D. Pei, W. J. Shi, S. K. Mo, P. Dudin, T. Kim, C. Cacho, G. Li, Y. Sun, L. X. Yang, Z. K. Liu, S. S. P. Parkin, C. Felser, and Y. L. Chen, Magnetic weyl semimetal phase in a kagome crystal, *Science* **365**, 1282 (2019).
- [31] F. H. Yu, T. Wu, Z. Y. Wang, B. Lei, W. Z. Zhuo, J. J. Ying, and X. H. Chen, Coexistence of anomalous hall effect and charge density wave in a superconducting topological kagome metal, *Phys. Rev. B* **104**, L041103 (2021).
- [32] G. Kresse and J. Furthmüller, Efficient iterative schemes for ab initio total-energy calculations using a plane-wave basis set, *Phys. Rev. B* **54**, 11169 (1996).
- [33] P. Giannozzi, S. Baroni, N. Bonini, M. Calandra, R. Car, C. Cavazzoni, D. Ceresoli, G. L. Chiarotti, M. Cococcioni, I. Dabo, A. Dal Corso, S. de Gironcoli, S. Fabris, G. Fratesi, R. Gebauer, U. Gerstmann, C. Gougoussis, A. Kokalj, M. Lazzeri, L. Martin Samos, N. Marzari, F. Mauri, R. Mazzarello, S. Paolini, A. Pasquarello, L. Paulatto, C. Sbraccia, S. Scandolo, G. Sclauzero, A. P. Seitsonen, A. Smogunov, P. Umari, and R. M. Wentzcovitch, Quantum espresso: a modular and open-source software project for quantum simulations of materials, *J. Phys.: Condens. Matter* **21**, 395502 (2009).
- [34] S. Baroni, S. de Gironcoli, A. Dal Corso, and P. Giannozzi, Phonons and related crystal properties from density-functional perturbation theory, *Rev. Mod. Phys.* **73**, 515 (2001).
- [35] F. Giustino, Electron-phonon interactions from first principles, *Rev. Mod. Phys.* **89**, 015003 (2017).
- [36] J. P. Perdew, K. Burke, and M. Ernzerhof, Generalized gradient approximation made simple, *Phys. Rev. Lett.* **77**, 3865 (1996).
- [37] G. Kresse and D. Joubert, From ultrasoft pseudopotentials to the projector augmented-wave method, *Phys. Rev. B* **59**, 1758 (1999).
- [38] Q. Wu, S. Zhang, H. F. Song, M. Troyer, and A. A. Soluyanov, Wanniertools: An open-source software package for novel topological materials, *Comput. Phys. Commun.* **224**, 405 (2018).
- [39] M. P. L. Sancho, J. M. L. Sancho, J. M. L. Sancho, and J. Rubio, Highly convergent schemes for the calculation of bulk and surface green functions, *J. Phys. F: Met. Phys.* **15**, 851 (1985).
- [40] N. Marzari, A. A. Mostofi, J. R. Yates, I. Souza, and D. Vanderbilt, Maximally localized wannier functions: Theory and applications, *Rev. Mod. Phys.* **84**, 1419 (2012).
- [41] I. Souza, N. Marzari, and D. Vanderbilt, Maximally localized wannier functions for entangled energy bands, *Phys. Rev. B* **65**, 035109 (2001).
- [42] C. Franchini, R. Kováčik, M. Marsman, S. Sathyanarayana Murthy, J. He, C. Ederer, and G. Kresse, Maximally localized wannier functions in LaMnO₃ within PBE + U, hybrid functionals and partially self-consistent gw: an efficient route to construct ab initio tight-binding parameters for eg perovskites, *J. Phys.: Condens. Matter* **24**, 235602 (2012).
- [43] See Supplemental Material for calculation details, phonon spectra of all MSn, band, DOS, band topology, and superconductivity for superconducting MSn.
- [44] W. L. McMillan, Transition temperature of strong-coupled superconductors, *Phys. Rev.* **167**, 331 (1968).
- [45] R. Dynes, Mcmillan's equation and the tc of superconductors, *Solid State Communications* **10**, 615 (1972).
- [46] P. B. Allen and R. C. Dynes, Transition temperature of strong-coupled superconductors reanalyzed, *Phys. Rev. B* **12**, 905 (1975).
- [47] X. Teng, J. S. Oh, H. Tan, L. Chen, J. Huang, B. Gao, J. X. Yin, J. H. Chu, M. Hashimoto, D. Lu, C. Jozwiak, A. Bostwick, E. Rotenberg, G. E. Granroth, B. Yan, R. J. Birgeneau, P. Dai, and M. Yi, Magnetism and charge density wave order in kagome FeGe, *Nature Physics* **19**, 814 (2023).
- [48] K. Kim, S. Kim, J. S. Kim, H. Kim, J.-H. Park, and B. I. Min, Importance of the van hove singularity in superconducting PdTe₂, *Phys. Rev. B* **97**, 165102 (2018).
- [49] H. Zhang, C. X. Liu, X. L. Qi, X. Dai, Z. Fang, and S. C. Zhang, Topological insulators in Bi₂Se₃, Bi₂Te₃ and Sb₂Te₃ with a single dirac cone on the surface, *Nat. Phys.* **5**, 438 (2009).
- [50] Y. S. Hor, A. J. Williams, J. G. Checkelsky, P. Roushan, J. Seo, Q. Xu, H. W. Zandbergen, A. Yazdani, N. P. Ong, and R. J. Cava, Superconductivity in Cu_xBi₂Se₃ and its implications for pairing in the undoped topological insulator, *Phys. Rev. Lett.* **104**, 057001 (2010).
- [51] T. Asaba, B. J. Lawson, C. Tinsman, L. Chen, P. Corbae, G. Li, Y. Qiu, Y. S. Hor, L. Fu, and L. Li, Rotational symmetry breaking in a trigonal superconductor nb-doped Bi₂Se₃, *Phys. Rev. X* **7**, 011009 (2017).
- [52] G. Balakrishnan, L. Bawden, S. Cavendish, and M. R. Lees, Superconducting properties of the substituted topological crystalline insulator SnTe, *Phys. Rev. B* **87**, 140507 (2013).
- [53] J. Hu, F. Yu, A. Luo, X. H. Pan, J. Zou, X. Liu, and G. Xu, Chiral topological superconductivity in superconductor-obstructed atomic insulator-ferromagnetic insulator heterostructures, *Phys. Rev. Lett.* **132**, 036601 (2024).
- [54] J. Hu, A. Luo, Z. Wang, J. Zou, Q. Wu, and G. Xu, A numerical method for designing topological superconductivity induced by s-wave pairing, *npj Computational Materials* **11**, 133 (2025).